CEST-KAN: Kolmogorov-Arnold Networks for CEST MRI Data Analysis

Jiawen Wang[1], Ziyan Wang[1], Pei Cai[1], Huabin Zhang[1], Jianpan Huang[1]*
[1] *Department of Diagnostic Radiology, The University of Hong Kong, Hong Kong, China.*
** Corresponding Author (jphuang@hku.hk).*

INTRODUCTION: CEST MRI is a promising molecular imaging technique that enables the in vivo detection of molecules.[1] However, its broad clinical application is impeded by the existing tedious post-processing methods, such as the frequently used, but time-consuming multi-pool Lorentzian fitting (MPLF) approach.[2,3] To address this issue, many deep learning techniques, mostly multi-layer perceptron (MLP) models, have been extensively applied to extract CEST metrics with fast speed in recently years.[4-9] Recently, Kolmogorov-Arnold Networks (KANs) have been proposed as promising alternatives to MLPs.[10] Unlike MLPs with fixed activation functions, KANs utilize learnable edge activations and spline-parametrized weights, leading to smaller yet more accurate models with faster scaling and enhanced interpretability (Fig. 1). In this study, we investigated the feasibility of using KANs in the analysis of CEST MRI data (CEST-KAN) and assessed the potential for clinical implementation of this method.

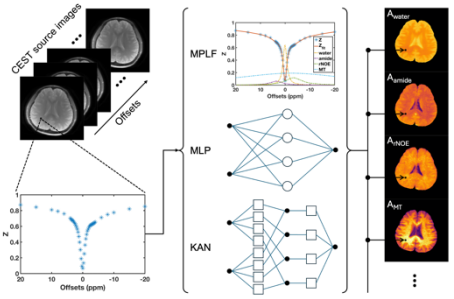

Fig. 1. Illustration of CEST maps generated by MPLF, MLP and KAN

METHODS: The study was approved by the local institutional review board and conducted according to the guidelines. CEST MRI experiments were performed at a 3T MRI system (SIGNA Premier, GE Healthcare) on six healthy volunteers (4 males and 2 females, aged 25-33 years old). The CEST sequence was a continuous wave (CW) module with a saturation time of 2 s and a saturation power of 0.8 μT, followed by a single-shot fast spin echo (FSE) readout module. An M_0 images at a frequency offset of −300 ppm and 43 CEST images at frequency offsets ranging from −20 to 20 ppm were acquired. Other parameters were as followings: TR = 3000 ms, slice thickness = 6 mm, reconstruction matrix size = 282×282 and FOV = 220×220 mm^2. CEST data from five subjects were used for training (131676 Z-spectra), while CEST data from one subject were reserved for testing (28102 Z-spectra). With reference to conventional MPLF method,[4,6,7] we compared the performance of MLP and KAN in generating multiple CEST contrasts, including water, amide, relayed nuclear Overhauser effect (rNOE) and magnetization transfer (MT) (Fig.1). The Z-spectra were used as input, while the MPLF fitting parameters were set as the output of the fitting/network model. To ensure a fair comparison, we set the network size and training parameters of MLP and KAN to be the same: [input size, hidden layer size, output size] = [43, 100, 9], training/validation data size = 0.8/0.2, learning rate = 0.01 (decays by a factor of 1/0.8 every epoch), early-stop patience = 50. Networks were trained on a computer equipped with an Intel(R) Core (TM) i9-13900KF Processor and an NVIDIA RTX4090 GPU.

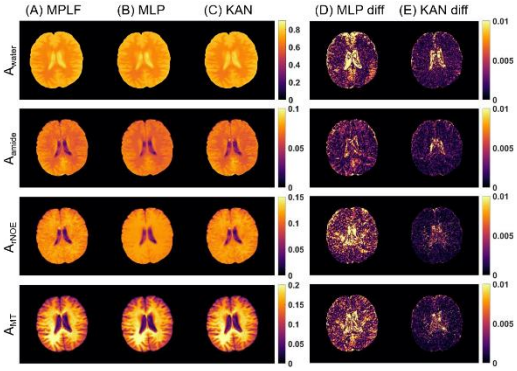

Fig. 2. Water/CEST maps created by (A) MPLF, (B) MLP and (C) KAN. Absolute difference maps between MPLF and (D) MLP or (E) KAN.

RESULTS & DISCUSSION: Fig. 2 displays the four water/CEST maps (A_{water}, A_{amide}, A_{rNOE}, and A_{MT}) generated by three methods. The water/CEST maps predicted by both MLP and KAN are visually comparable to the results obtained using MLPF (Fig. 2A-C). However, KAN demonstrates higher accuracy than MLP, as evidenced by the smaller error displayed in the absolute difference maps (Fig. 2D&E). To quantitatively compare the accuracy of MLP and KAN, we performed voxel-by-voxel correlation analysis of the four metrics between MLP/KAN and MPLF. As shown in Fig. 2, all the four metrics generated by KAN exhibit higher Pearson coefficients when compared to the MLP results (R = 0.996 vs 0.989, 0.956 vs 0.937, 0.988 vs 0.942, and 0.997 vs 0.990 for A_{water}, A_{amide}, A_{rNOE}, and A_{MT}, respectively). These results support the findings presented in Fig. 2. KAN outperform MLP in CEST MRI data analysis probably due to its unique architecture, which combines the strengths of splines and neural networks. Splines are highly accurate in modeling low-dimensional functions, while neural networks excel in learning compositional structures. This combination can effectively capture local details and global patterns in CEST data, resulting in improved modeling accuracy. Further investigation using a larger dataset is underway to validate these findings.

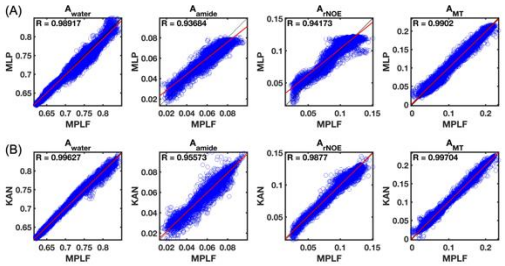

Fig. 3. Correlation results of MPLF with (A) MLP and (B) KAN in water/CEST contrasts.

CONCLUSION: In this study, we demonstrate the feasibility of utilizing KAN for CEST MRI data analysis, highlighting its superiority over MLP in the same task. The findings suggest that CEST-KAN has the potential to be a robust and reliable post-analysis tool for CEST MRI in clinical settings.

ACKNOWLEDGMENTS: The University of Hong Kong: 109000487, 204610401 and 204610519.

REFERENCES: 1. P. C. van Zijl, N. N. Yadav. Magn Reson Med 2011;65:927. **2.** Zaiß, *et al*. J Magn Reson 2011;211:149-155. **3.** Jones CK., *et al.* Neuroimage 2013;77:114. **4.** Zaiss M, *et al.* Magn Reson Med 2019;81:3901. **5.** Chen L, *et al.* Nat Commun 2020;11:1072. **6.** Glang F, *et al.* Magn Reson Med 2020;84:450. **7.** Huang J, *et al*. Magn Reson Med 2022;87:1529. **8.** Perlman O *et al*. Nat Biomed Eng, 2022;6:648. **9.** Kim B, *et al*. Neuroimage, 2020;221:117165. **10.** Liu Z, *et al.* arXiv preprint arXiv:2404.19756 2024.